Baseline OCT Measurements in the Idiopathic Intracranial Hypertension Treatment Trial, Part I: Quality Control, Comparisons, and Variability

OCT Sub-Study Committee for the NORDIC Idiopathic Intracranial Hypertension Study Group

Icahn School of Medicine at Mount Sinai, NORDIC Headquarters, New York, New York, United States

Correspondence: Mark J. Kupersmith, Icahn School of Medicine at Mount Sinai, NORDIC Headquarters, 1000 10th Avenue, New York, NY 10019, USA; mkuper@chpnet.org.

See the appendix for the members of the OCT Sub-Study Committee for the NORDIC Idiopathic Intracranial Hypertension Study Group.

Submitted: June 5, 2014
Accepted: October 13, 2014

Citation: OCT Sub-Study Committee for the NORDIC Idiopathic Intracranial Hypertension Study Group. Baseline OCT measurements in the Idiopathic Intracranial Hypertension Treatment Trial, part I: quality control, comparisons, and variability. *Invest Ophthalmol Vis Sci*. 2014;55:8180–8188. DOI:10.1167/iovs.14-14960

Purpose. Optical coherence tomography (OCT) has been used to investigate papilledema in single-site, mostly retrospective studies. We investigated whether spectral-domain OCT (SD-OCT), which provides thickness and volume measurements of the optic nerve head and retina, could reliably demonstrate structural changes due to papilledema in a prospective multisite clinical trial setting.

Methods. At entry, 126 subjects in the Idiopathic Intracranial Hypertension Treatment Trial (IIHTT) with mild visual field loss had optic disc and macular scans, using the Cirrus SD-OCT. Images were analyzed by using the proprietary commercial and custom 3D-segmentation algorithms to calculate retinal nerve fiber layer (RNFL), total retinal thickness (TRT), optic nerve head volume (ONHV), and retinal ganglion cell layer (GCL) thickness. We evaluated variability, with interocular comparison and correlation between results for both methods.

Results. The average RNFL thickness > 95% of normal controls in 90% of eyes and the RNFL, TRT, ONH height, and ONHV showed strong ($r > 0.8$) correlations for interocular comparisons. Variability for repeated testing of OCT parameters was low for both methods and intraclass correlations > 0.9 except for the proprietary GCL thickness. The proprietary algorithm–derived RNFL, TRT, and GCL thickness measurements had failure rates of 10%, 16%, and 20% for all eyes respectively, which were uncommon with 3D-segmentation–derived measurements. Only 7% of eyes had GCL thinning that was less than fifth percentile of normal age-matched control eyes by both methods.

Conclusions. Spectral-domain OCT provides reliable continuous variables and quantified assessment of structural alterations due to papilledema. (ClinicalTrials.gov number, NCT01003639.)

Keywords: papilledema, intracranial hypertension, optical coherence tomography, OCT

Idiopathic intracranial hypertension (IIH) is a disorder that affects overweight women of childbearing age,[1,2] with a rising incidence in parallel with the current obesity epidemic in the United States.[3] Patients have headaches, pulsatile tinnitus, transient visual obscurations, and diplopia in association with optic disc edema (papilledema). Some degree of vision loss occurs in 86% of patients and 10% develop severe visual loss.[2] The effectiveness of treatment had not been verified by properly designed clinical trials until the implementation of the Idiopathic Intracranial Hypertension Treatment Trial (IIHTT), sponsored by the National Eye Institute. This trial has shown that acetazolamide plus weight management improves the visual fields more than weight management plus placebo at the 6-month study outcome.[4]

The accepted objective method for evaluating papilledema and monitoring the alterations in the optic nerve head (ONH) is the Frisén scale, a noncontinuous ordinal grading based on specific features described in fundus photographs or on ophthalmoscopy.[5] The scale has been clinically useful but lacks sensitivity to small changes in the degree of disc edema and varies among observers.[6,7] In contrast, optical coherence tomography (OCT) measurement of the peripapillary retina nerve fiber layer (RNFL) thickness provides a continuous quantitative assessment of papilledema that correlates with Frisén grading.[6,8,9] Typically, OCT assessments are used to evaluate thinning of the RNFL due to optic nerve injury from many causes.[10–12] Although prior smaller studies of IIH have shown that lower-resolution time-domain OCT imaging of the RNFL thickness can monitor changes in papilledema over time,[13,14] other studies[15] suggest the commercially available algorithms used in both time-domain and newer spectral-domain (SD) OCT units to calculate RNFL thickness can be unreliable and fail with severe papilledema (Mandel G, et al. *IOVS* 2010;51:ARVO E-Abstract 555).

The OCT substudy of the IIHTT was designed to systematically explore potential continuous measures of alterations in the structures of the ONH and macula due to papilledema, and monitor changes in the ONH, peripapillary and macular retinal layer thicknesses during treatment. Since the SD-OCT instrument and proprietary two-dimensional segmentation software methods are not designed to measure swelling of the ONH or the peripapillary retina, we evaluated a variety of approaches via a pilot study. We explored SD-OCT parameters and procedures that could be applied across multiple study sites to provide uniform data collection that measured the effects of papilledema (see Supplementary Appendix Pilot study file). In

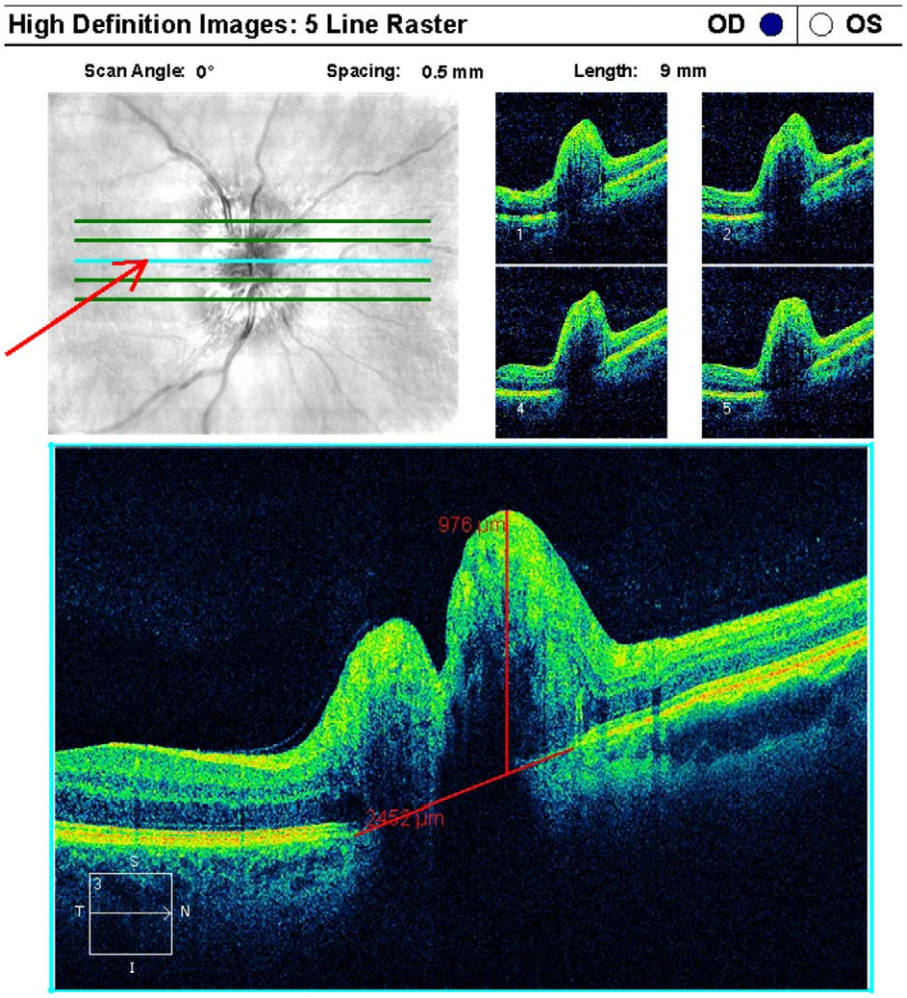

FIGURE 1. High-definition five-line raster through the ONH showing the difficulty in including the entire vertical dimensions of the swollen optic disc. For each raster line, the ONH elevation was measured by manually placing a vertical line from a line connecting the RPE layer temporal and nasal neural canal borders to the top of the ONH.

the pilot study, we investigated eyes with ONH swelling of patients not in the IIHTT. The pilot study data showed that all of the measures detailed in Methods were reproducible and reliable (see Supplementary Appendix Pilot study file), and the results were used to develop the final study protocol. In this report, we describe the following: (1) IIHTT OCT substudy protocol; (2) IIHTT OCT substudy baseline data, including interocular and intraclass correlations (ICCs) and comparisons; and (3) comparison of measurements obtained by a proprietary commercially available algorithm and a three-dimensional (3D)–segmentation algorithm[16] for each SD-OCT parameter obtained at baseline. In part II, we describe the relationship of SD-OCT features to other measures relevant to IIH, including the Frisén grading scale and measures of visual performance, which was studied for the duration of the IIHTT and the continuation observational study currently in progress.

METHODS

Details of the IIHTT study design and entry criteria are published.[17] Newly diagnosed IIH patients naïve to treatment with a perimetric mean deviation (PMD) of –2.00 to –7.00 dB using the SITA standard 24-2 test pattern on the Humphrey Field Analyzer II perimeter (Swedish Interactive Threshold Algorithm; Carl Zeiss Meditec, Inc. [ZM], Dublin, CA, USA) in the worse eye ("study eye") were enrolled. All subjects signed consent and the study was performed under institutional review board approval. Standardized fundus photography, Frisén grading of photos at the photographic reading center and by clinical examination by site investigators, high- and low (2.5%)–contrast visual acuity measurements, threshold 24-2 perimetry, and SD-OCT imaging, using the Cirrus 4000 SD-OCT (6.01 software; ZM), were performed in each eye at each visit. Study sites followed a study-specific protocol for image collection by certified technicians, digitally transferred the collected data, and performed quality control and analyses through the OCT Reading Center (OCTRC), experienced in evaluating optic nerve and RNFL thickness determinations. The entire study was approved by multiple IRBs and subjects signed informed consent in compliance with the Declaration of Helsinki.

SD-OCT Scan Procedure

The image acquisition protocol required three different types of OCT scans: (1) one high-definition (HD) five-line raster scan horizontally oriented, separated by 0.5 mm (each scan 9 mm in length) and spread across the entire surface of the optic disc (Fig. 1), two optic disc area 200 × 200 volume scans centered on the optic disc, and two macula area 200 × 200 volume scans

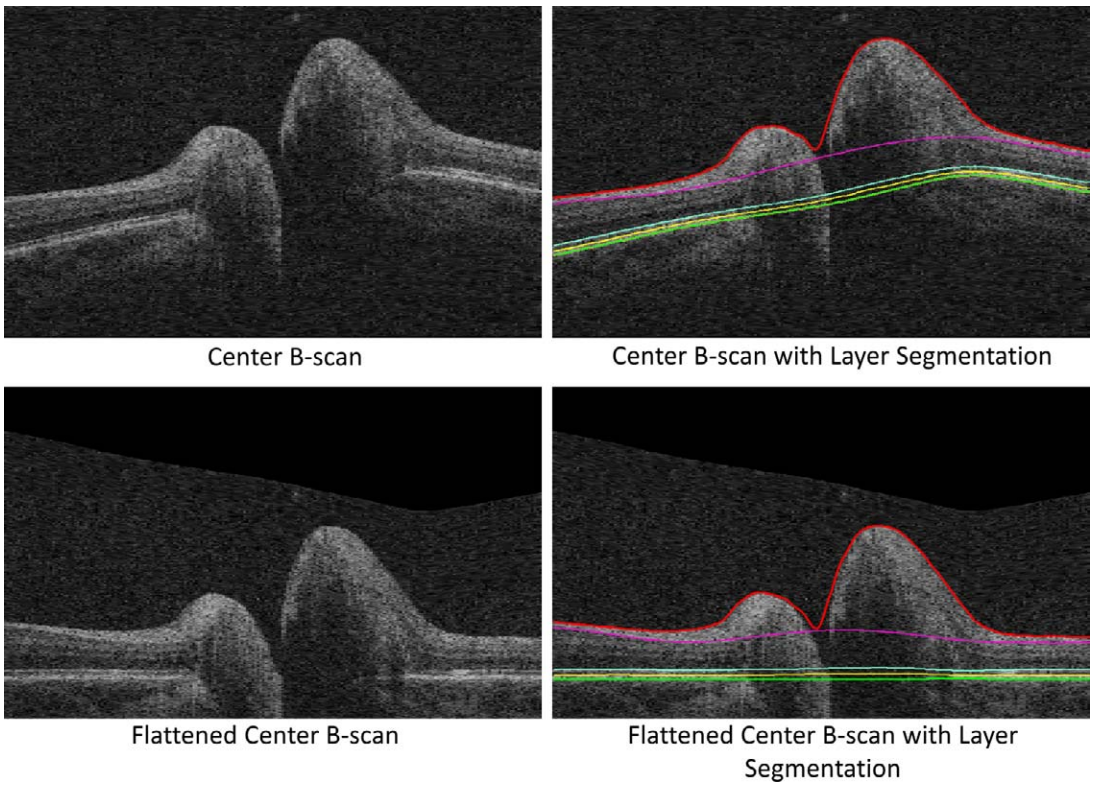

FIGURE 2. Three-dimensional segmentation of the ONH region volume scan. *Top*: Actual axial images. *Bottom*: Images flattened to allow 3D segmentation. *Red line* defines internal limiting membrane. *Yellow lines* follow Bruch's membrane and RPE. *Pink line* defines the RNFL layer border.

centered on the fovea. Scans were acquired from both eyes at baseline and at months 3, 6, 12, 24, 36, and 48. The OCT data were uploaded to the NORDIC Imaging Center site via a secure upload Web client. In addition to certifying site equipment and technicians, the OCTRC maintained quality control on all OCT data collected by using a protocol that addressed three areas of technician performance (see Supplementary Material for details): (1) test parameter errors, (2) patient data errors, and (3) shipment errors. Test parameter errors included poor alignment, signal strength < 7, wrong scan used, and missing scans.

SD-OCT Parameters Calculated

The OCT measures were chosen to reflect swelling of the ONH or papillary retina or structural loss of RNFL or retina ganglion cells due to papilledema.

Using the optic disc area images, we calculated the average RNFL thickness value by using the software provided with the Cirrus machine and external software package to export and process data (Research Browser; ZM). The average total peripapillary circumference retinal thickness (TRT) was calculated from an internal analysis program at ZM that used the same radius as that used for the RNFL.

The optic disc area images were also evaluated at the University of Iowa, by using 3D analysis of segmented optic disc volume scans (Fig. 2), to calculate the average RNFL and TRT thickness and ONH volume values. Three-dimensional segmentation uses all neighboring image information and not just in each B-scan.[16] Layer segmentation was performed on the ONH-centered scans and 3D volumetric parameters were computed as follows: from each ONH-centered volume, the total retinal volume (i.e., the volume between the internal limiting membrane and the retinal pigment epithelium [RPE] reference surface) was computed. The RNFL and TRT thicknesses were computed using a radius of 1.73 mm around the center of the optic nerve head.

Using the macular area volumetric images, we measured the total retinal thickness of sectors and the average thickness of the ganglion cell layer and inner plexiform layer complex (GCL+IPL) by using the ZM proprietary software and Research Browser. This method finds the distance between the outer boundary of the RNFL and the outer boundary of the IPL to report the combined thickness of the GCL+IPL, while excluding the RNFL.[18] The average, minimum (lowest GCL+IPL thickness over a single meridian crossing the annulus), and sectoral (superotemporal, superior, superonasal, inferonasal, inferior, inferotemporal) thicknesses were measured in an elliptical annulus (standard dimensions for ZM software analysis: vertical inner and outer radius of 0.5 and 2.0 mm, respectively; horizontal inner and outer radius of 0.6 and 2.4 mm, respectively) around the fovea. The size of the inner ring was chosen to exclude the area where the GCL is thin and difficult to detect, whereas the dimension of the outer ring was selected to conform closely to the real anatomy of the macular region, and where the GCL is thickest in a normal eye. The input image data are initially divided by using the inner limiting membrane and RPE identification algorithms to create a region of interest within the intraretinal layers. The algorithm sequentially segments the outer boundary of the outer plexiform layer first, the outer boundary of the IPL next, and the outer boundary of the RNFL last. The boundary between GCL and IPL is difficult to visualize in the image data so the algorithm measures GCL+IPL thickness.

Three-dimensional–segmentation analysis was also used to measure the average GCL+IPL thickness across the macular

Table 1. Description (Quartiles, Limits) of the Measures Studied Based on the First Measure of the Study Eye (Worse Eye)

Label	N	Lower Quartile	Median	Upper Quartile	Mean	Std Dev	Minimum	Maximum
ZM algorithm–calculated measures								
Average RNFL, μm	122	135.2	220.9	356.8	256.8	137.4	76.3	621.2
Average TRT, μm	126	372.7	473.1	610.3	504.9	167.3	264.3	982.6
Average GCL+IPL, μm	126	73.0	83.0	88.0	76.4	18.7	28.0	104.0
Center fovea macular thickness, μm	125	237.0	250.0	265.0	251.3	22.0	197.0	310.0
Inner nasal macular thickness, μm	125	306.0	321.0	332.0	319.6	18.5	281.0	373.0
Outer nasal macular thickness, μm	125	260.0	274.0	285.0	273.7	19.5	232.0	329.0
3D-segmentation algorithm–calculated measures								
Average RNFL, μm	122	134.2	213.7	388.6	274.0	166.7	71.1	703.6
Average TRT, μm	122	372.2	477.5	675.7	540.4	207.4	272.2	1061.1
Average GCL+IPL, μm	124	80.7	85.8	89.8	85.2	7.1	65.8	103.1
Average GCL as percentile of ZM controls, %	124	24.9	58.2	82.5	53.7	31.4	0.1	99.9
Total volume ONH, mm^3	122	13.6	15.6	19.1	16.5	3.8	10.5	25.9
Line 3 of raster lines, μm	120	855.5	998.5	1141.0	999.7	224.9	516.0	1528.0

Line 3 (the middle of the five HD raster lines) ONH height is displaced rather than for all five lines. Std Dev, standard deviation.

region. Eleven intraretinal surfaces of each macula-centered volumetric scan were first segmented by using the graph-theoretic approach developed at the University of Iowa.[15,16] The following surfaces were retained to enable computation of the fovea center and GCL+IPL thickness: (1) the internal limiting membrane, (2) the interface between the RNFL and the GCL, (3) the interface between the IPL and the inner nuclear layer, and (4) the posterior surface of the RPE layer. For each A-scan location, the GCL+IPL thickness was defined as the distance between the second surface and the third surface. The mean GCL+IPL thickness was computed within an elliptical annulus (with a vertical inner and outer radius of 0.5 and 2.0 mm, respectively; and horizontal inner and outer radius of 0.6 and 2.4 mm, respectively) centered at the fovea.

A final method generated ONH elevation values for the five HD raster line sections. For each raster line image through the ONH, a horizontal line was electronically drawn connecting the visible RPE/Bruch's membrane layer demarcating the temporal and nasal borders of the neural canal of the ONH. The maximal height of ONH elevation was electronically measured from this line to the maximal elevation of the ONH (Fig. 1). An average ONH height was calculated from the values for each of the five lines. If the RPE temporal or nasal border was outside the imaging window in any of the five raster lines (this occurred with severe papilledema), then the largest ONH height measurement made within the window was taken for that line. The five-line raster parameter was chosen for two reasons: (1) the HD five-line raster images will be used in future shape analysis of the ONH[19,20]; and (2) the pilot study showed the reliability of this parameter (see Supplementary Appendix Pilot study), and at the start of the IIHTT this was the only available method that could be related to the ONH volume.

Analyses

The SD-OCT measurements were performed twice for each eye; however, the five-line raster scan was performed once for each eye. For the five-line raster scan, the height from line 3 (most centered on the ONH and the average height for of all five lines) was used for analyses. For 3D-segmentation GCL+IPL thickness, age-matched controls (derived by 3D segmentation of the set of normative scans provided by ZM) were used to determine the average GCL as a percentile of the controls. Quality control assessments of all baseline scans were summarized by type of error (see Supplementary Appendix OCTRC Activities). Descriptive statistics were used to summarize each SD-OCT measure based on the first measurement of the study eye (the eye with worse PMD). The first SD-OCT measures from both eyes were compared by using Pearson correlation coefficients to describe the interocular relationship of these measures (each comparison was for the same parameter and method of analysis performed in both eyes). The variability of repeated measurements in the same eye was assessed by (1) determining the difference in the measures between the two scans and summarizing this difference by using descriptive statistics and (2) calculating ICC coefficients.

The GCL+IPL value calculated by 3D segmentation was defined as thinned if the study eye GCL value was below the fifth percentile of the 3D-segmentation GCL value derived from age-matched Zeiss normative scans. *t*-tests were used to compare this group to study subjects with GCL+IPL thickness values equal to or above the fifth percentile of controls with regard to the mean inner and outer nasal sectors of macular TRT, to see if any early thinning might be due to edema in the retina.

Results

We enrolled 126 subjects, 122 women and 4 men, at 24 sites in the OCT substudy of 165 subjects enrolled in the IIHTT. Spectral-domain OCT imaging was performed by certified technicians. Technical issues (due to protocol compliance or severity of ONH swelling precluding adequate OCT imaging and centering) resulted in rejection of 2.7% of OCT data (see Quality Control Assessment in Supplementary Appendix OCTRC Activities).

The average RNFL thickness derived from the ZM proprietary algorithm was above the 95% percentile of the normal Cirrus controls in 220 eyes (90%). The SD-OCT measurements for each parameter reflecting swelling of the optic nerve head and retina, RNFL, TRT, and ONH volume, regardless of whether the values were derived with the ZM proprietary or 3D-segmentation algorithm, showed a wide range of values among study eyes (Table 1). The GCL+IPL thickness values, calculated from the 3D-segmentation algorithm, had a narrower range of values and standard deviation than the ZM algorithm GCL+IPL measurements (see below). The variability for all SD-OCT parameters, performed twice for all eyes at baseline, was low (Table 2).

Interocular comparisons for ZM proprietary and 3D-segmentation algorithms, used to derive RNFL, average TRT,

Table 2. Description of Interocular Correlations and Differences on Repeated OCT Measures for All Eyes

Label	Lower Quartile	Median	Upper Quartile	Mean	Std Dev	Std Error	Interocular Correlation Coefficient*	ICC Study Eyes*	ICC Nonstudy Eyes*
ZM algorithm–derived measures									
Average RNFL, μm	−6.16	0.07	4.60	−1.60	22.4	1.40	0.85	0.99	0.99
Average TRT, μm	−2.44	0.35	3.92	−0.88	35.5	2.20	0.74	0.94	0.93
Average GCL+IPL, μm	−1.0	0	1.0	−0.51	10.5	0.66	0.96	0.86	0.75
3D-segmentation algorithm–derived measures									
Total volume ONH, mm^3	−0.05	0.01	0.09	−0.01	0.79	0.04	0.85	0.99	0.99
Average RNFL, μm	−4.25	−0.38	3.98	0.44	13.3	0.82	0.85	0.99	0.99
Average TRT, μm	−4.18	−0.16	4.46	0.42	22.9	1.44	0.86	0.99	0.99
Average GCL+IPL, μm	−0.32	0.08	0.39	0.36	4.9	0.31	0.88	0.99	0.99

Intraclass correlations for study and fellow, nonstudy eyes on repeated measures. Interocular differences were calculated as right eye minus left eye so values could be positive or negative.

* All correlations had $P = 0.01$.

ONH volume, and GCL+IPL values, showed strong correlation for all SD-OCT parameters (Table 2; see Supplementary Appendix Figs. Sa–Sd). Interocular correlations for the ONH height assessed by the middle line, raster line 3 ($r = 0.72$, $P = 0.01$), and for the average value measured for all five lines ($r = 0.75$, $P = 0.01$), were also high.

The ZM algorithm, but not the 3D-segmentation algorithm, appeared to fail in 12 eyes for RNFL thickness (we defined failure as having RNFL thickness values greater than the ZM standard deviation for all eyes with RNFL, 137 μm less than the corresponding 3D-segmentation values) and in 19 eyes for TRT (we defined failure as having TRT values greater than the ZM standard deviation for all eyes with TRT, 167 μm less than the corresponding 3D-segmentation values) measurements when the swelling or thickness measurements were at the higher levels (Figs. 3–5). Of 252 eyes, four (four study eyes) in four subjects had 3D-segmentation failure to calculate values for the RNFL thickness, TRT, and ONH volume (see Discussion for reasons). Despite the failures, there was strong correlation for the 3D-segmentation– and ZM algorithm–derived measurements for average RNFL ($r = 0.91$, $P = 0.01$) and TRT ($r = 0.87$, $P = 0.01$) thickness for all eyes (Figs. 3, 4).

Early in the study, the OCTRC quality control evaluation showed a major disparity between the two methods, suggesting GCL+IPL thinning by the ZM proprietary method could be due to artifact. The amount of thinning by the proprietary ZM method was extreme in some eyes (Table 1, minimum and standard deviation results; Fig. 5). We then determined that if only one method showed that the baseline GCL+IPL thickness was below the fifth percentile of controls, it would be considered an algorithm failure (see Discussion for rationale). The ZM algorithm showed that the GCL+IPL thickness measurements were below the fifth percentile of controls in 34 study eyes (and in 50 of all 252 eyes) in contrast to 9 study eyes, using the 3D segmentation. All nine eyes (none had GCL+IPL less than 65 μm) showing thinning by 3D segmentation also showed thinning by the ZM algorithm, and the average difference for both methods was less than 5 μm. Of the 34 study eyes showing abnormal thinning by the proprietary ZM method, 25 did not show thinning by 3D segmentation and were consequent to algorithm "failure," based on inspection of the segmentation boundaries superimposed on B-scans and values typically ≥30 μm less than the corresponding 3D-segmentation–derived values. These 34 eyes had mean 3D-

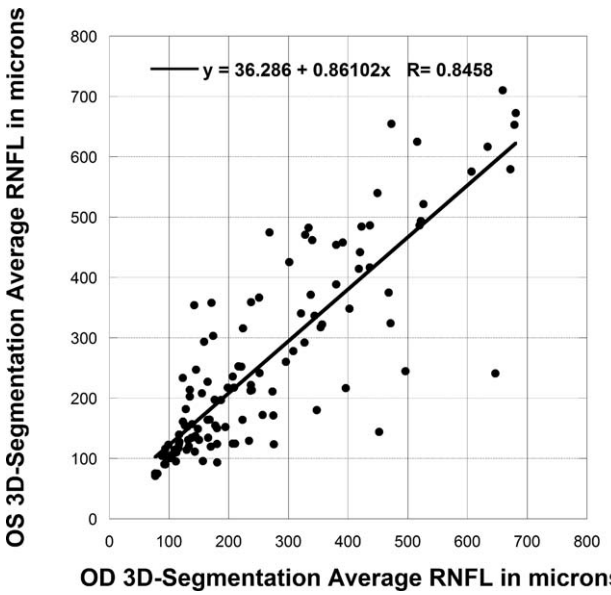

Figure 3. Three dimensional segmentation compared to ZM calculations for average RNFL thickness.

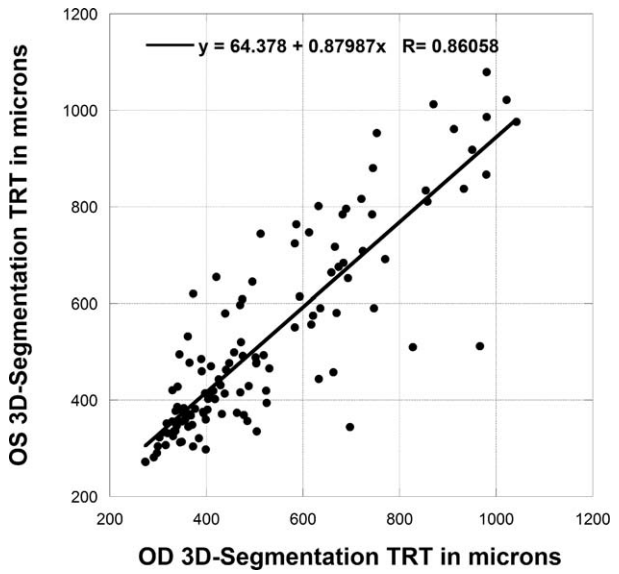

Figure 4. Three-dimensional segmentation compared to ZM calculations for average TRT.

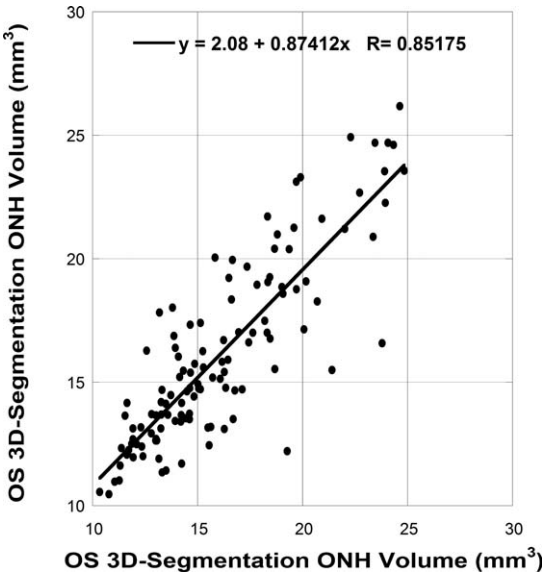

FIGURE 5. Three-dimensional segmentation compared to ZM calculations for average GCL+IPL thickness.

segmentation values for average RNFL (385 ± 185 μm), average TRT (683 ± 227 μm), and ONH volume (19.2 ± 3.9 μm^3) that were significantly increased compared with average RNFL (227 ± 131 μm, $P = 0.001$), average TRT (482 ± 165 μm, $P = 0.001$), and ONH volume (15.4 ± 3.1 mm^3, $P = 0.001$) for the remaining 88 study eyes, in which the ZM algorithm appeared not to fail.

DISCUSSION

The OCT IIHTT substudy showed that reliable, consistent, quality OCT data can be collected for IIH patients with papilledema from multiple sites with commercially available SD-OCT machines. The OCTRC procedures and methodology for the collection and digital transfer of uniform spectral SD-OCT generated quality data collected at each site, using the same OCT equipment with a standardized protocol, certified technicians, quality control of data, and data analysis. Only 2.9% of the baseline OCT images were determined to be unusable owing to incorrect data acquisition. The HD five-line raster scan had the most errors, usually due to the wrong scan parameters being chosen for scan acquisition. This was likely due to the protocol requirement for specific parameters, which differed from the default settings. Prompt transmission of OCT data via a secure Internet-accessible file transfer protocol to the OCTRC allowed rapid quality control monitoring and feedback to sites, which reduced the frequency of errors.[21] The success of this study, which used 24 sites naïve to SD-OCT data collection, shows the utility of an OCTRC.[22–27]

Interocular correlations for all SD-OCT parameters reflecting papilledema-related swelling in the ONH or peripapillary retina were highly significant. The OCT continuous variable measures showed that most IIH patients, with newly diagnosed disease and mild visual field loss (PMD range, −2.00 to −7.00 dB), have relatively symmetrical amounts of papilledema. In contrast, prior studies using the Frisén grade have suggested that a markedly asymmetric papilledema occurs in approximately 10% of all IIH patients. These studies,[28] however, include a more heterogeneous population with respect to the duration of symptoms and the amount of visual field loss at the time of testing. Further, our findings support the supposition that truly unilateral papilledema is rare.[29,30] Given the ease of imaging of both eyes and the potential for possible asymmetric change over time, we do not recommend imaging only one eye.

In clinical practice, SD-OCT data are typically presented and analyzed by using the proprietary algorithms provided by the device manufacturer device, which are specifically designed to evaluate thinning of the RNFL due to glaucoma, not thickening due to edema. Prior reports indicate that SD-OCT proprietary algorithms for RNFL thickness measurement can fail,[15] particularly when the RNFL > 200 μm due to papilledema (Mandel G, et al. *IOVS* 2010;51:ARVO E-Abstract 555). We found similar distortions of company-derived measurements of the TRT. Company proprietary algorithms to measure retinal ganglion cell layer thickness may also fail when there is significant ONH swelling, resulting in the erroneous appearance of GCL+IPL thinning in 20% of IIHTT study eyes. We previously have reported similar errors in patients with optic disc edema due to anterior ischemic optic neuropathy and optic neuritis (Kupersmith MJ, et al. *IOVS* 2013;54:ARVO E-Abstract 3233). This problem may also be an issue in other commercial SD-OCT devices. The commercial methods may be more susceptible to artifacts because they were not designed to evaluate patients with disc edema where the normal architecture of retinal borders is obscured. These two-dimensional segmentation methods assume a quantitative relationship between the internal limiting membrane and the outer layers of the retina and segment each B-scan independently. In fact, the user manual recommends that the user visually inspect the image to determine if the segmentation lines are correctly positioned along the inner boundary of the GCL and outer boundary of the IPL. Thus, this method appears to be more susceptible to failure with any process, such as edema due to swelling of the peripapillary RNFL and adjacent retina, which disrupts the regular retinal layer position or shape or boundaries. We hypothesized that these failures could

TABLE 3. Description (Quartiles, Limits) of Nasal Sectors of Macular TRT for Study Eyes With GCL-IPL Thickness Values Either Below the Fifth Percentile or Equal to or Above the Fifth Percentile of ZM Controls by 3D Segmentation

	N	Lower Quartile	Median	Upper Quartile	Mean	Std Dev	Minimum	Maximum
Inner sector nasal retinal thickness								
Eyes with GCL+IPL < 5%	9	282.0	301.0	311.0	299.2	14.3	281.0	317.0
Eyes with GCL+IPL ≥ 5%	115	308.0	322.0	333.0	321.1*	18.0	282.0	373.0
Outer sector nasal retinal thickness								
Eyes with GCL+IPL < 5%	9	237.0	249.0	260.0	250.6	15.2	232.0	276.0
Eyes with GCL+IPL ≥ 5%	115	261.0	275.0	285.0	275.4†	18.7	241.0	329.0

* $P = 0.001$.
† $P = 0.0002$.

arise from edema or disorganization of retinal layers due to retinal swelling. We tested this hypothesis by exploring the nasal sectors in the macular scan, since the proximity to the optic disc swelling would have the highest chance of affecting this region. However, eyes with GCL+IPL thickness values below the fifth percentile of controls, when using either the commercial (data not shown) or 3D-sementation algorithm (Table 3), did not have thicker TRT in the nasal sectors of the macular scan (papillomacular region) than eyes without reduced GCL+IPL thickness. This suggests this failure may be due to alterations in the peripapillary region.

In contrast, the 3D-segmentation method incorporates contextual information to optimize the process and thus reduce failures due to local distortions in retinal layers. In the IIHTT study, the 3D segmentation did not fail for GCL measurement except in 0.8% of eyes where the macular region images were not adequate (off center or wrong region). Similarly, 3D segmentation of the ONH fails infrequently (in approximately 2.4% of IIHTT eyes), but it can falter if Bruch's membrane and the RPE layer in the peripapillary retina cannot be identified, whether due to poor signal penetrance through edematous inner retinal layers or if excluded from the scan boundary. This can also prevent accurate manual measurement of the ONH height using the HD five-line raster images. The 3D-segmentation methodology used in this study appears to be reliable and less prone to failure in evaluating the GCL, ONH, and peripapillary retina and layers of retina in the papillomacular region that have structural changes due to ONH swelling.[15,16]

Given that study eyes had visual field loss at baseline, albeit mild, we anticipated that some degree of GCL thinning would be common. Using 3D segmentation, compared with age-matched controls provided from ZM, only 7.3% of study eyes had macular region GCL+IPL thinning (<fifth percentile) at baseline. Our results suggest that in patients with newly diagnosed IIH and mild vision loss, detectable thinning or loss of retinal ganglion cells is infrequent.

We included the five-line HD raster line program, originally designed to study retinal layers in the macula, to the study protocol in order to explore alterations in shape of the ONH and the neural canal bordered by Bruch's membrane and the RPE, due to papilledema.[19,20] Because the five-line raster scan averages a number of B-scans for each raster line, the signal is improved, especially in locations affected by edema. The ONH shape results have not been analyzed and are pending completion of automation of the 3D-segmentation method to perform this analysis. However, we did use the raster images to successfully measure the ONH height manually, which correlate with the 3D-segmentation method measurement of peripapillary retinal thickening and ONH volume. Until commercial algorithms to calculate ONH volume become available, measuring ONH height manually is another measure for following ONH swelling due to papilledema.

It remains to be determined whether eyes with reduced GCL+IPL thickness at baseline will have worse vision or greater RNFL thinning over time. The GCL+IPL thinning might reflect optic nerve injury, while the ONH and RNFL swelling persists and prevents early identification of RNFL loss. We have not fully analyzed the macular images to determine the nature and frequency of alterations in the outer retinal layers, which might be a cause of early vision dysfunction. As in ONH alterations, outer retinal changes might be reversible as treatment lowers the intracranial hypertension, but only the follow-up data will show whether some permanent structure changes occur in some or all retinal layers.

In a prior report using time-domain OCT, children with IIH appear to have selective thickening of the nasal macula in the papillomacular region.[31] Given the proximity of this region to the swollen ONH, we also anticipated we would find this. In contrast, the IIHTT subjects with mild visual field loss had no eyes with thickening of either the inner or outer nasal total retinal paramacular region, compared with corresponding temporal area and the temporal regions. In fact, the temporal regions were frequently thicker. There was no significant difference between outer temporal (299 ± 34 μm) and nasal (271 ± 18 μm) regions and inner temporal (326 ± 17 μm) and nasal (317 ± 14 μm) macular thickness values.

Currently available SD-OCT methods of imaging the ONH and macula appear to produce reliable data, which can be used to investigate the effects of papilledema on the ONH and retina. It is clinically important to carefully evaluate algorithm performance in SD-OCT scans, since failures may lead to false interpretations of data and may adversely influence clinical decisions. Three-dimensional segmentation–based applications appear to be superior to commercially available 2D algorithms for calculating thickness of RNFL, TRT, and GCL. Analysis of these measures, correlation with acetazolamide use, weight loss, and change in lumbar puncture–determined opening pressure will be reported after the primary outcome of the IIHTT are analyzed and reported.

Acknowledgments

Supported by Grants U10 EY017281-01A1, U10 EY017387-01A1, and 3U10EY017281-01A1S1.

Disclosure: **M.J. Kupersmith**, None

References

1. Corbett J, Savino P, Thompson H, et al. Visual loss in pseudotumor cerebri: follow-up of 57 patients from five to 41 years and a profile of 14 patients with permanent severe visual loss. *Arch Neurol*. 1982;39:461–474.
2. Wall M, George D. Idiopathic intracranial hypertension: a prospective study of 50 patients. *Brain*. 1991;114:155–180.
3. Garrett J, Corbett JJ, Braswell RA, Santiago M. The increasing incidence of IIH. The effect of obesity on frequency of occurrence in Mississippi. *Ann Neurol*. 2004;56(suppl 8): S69.
4. The NORDIC Idiopathic Intracranial Hypertension Study Group. Effect of acetazolamide on visual function in patients with idiopathic intracranial hypertension and mild visual loss: the Idiopathic Intracranial Hypertension Treatment Trial. *JAMA*. 2014;311:1641–1651.
5. Frisén L. Swelling of the optic nerve head: a staging scheme. *J Neurol Neurosurg Psychiatr*. 1982;45:13–18.
6. Scott C, Kardon R, Lee A, Frisén L, Wall M. Diagnosis and grading of papilledema in patients with raised intracranial pressure using optical coherence tomography vs clinical expert assessment using a clinical staging scale. *Arch Ophthalmol*. 2010;128:705–711.
7. Sinclair A, Burdon M, Nightingale P, et al. Rating papilloedema: an evaluation of the Frisén classification in idiopathic intracranial hypertension. *J Neurol*. 2012;259:1406–1412.
8. Echegaray S, Zamora G, Yu H, Luo W, Soliz P, Kardon R. Automated analysis of optic nerve images for detection and staging of papilledema. *Invest Ophthalmol Vis Sci*. 2011;52: 7470–7478.
9. Tang L, Kardon RH, Wang JK, Garvin MK, Lee K, Abramoff MD. Quantitative evaluation of papilledema from stereoscopic color fundus photographs. *Invest Ophthalmol Vis Sci*. 2012; 53:4490–4497.
10. Schuman JS, Hee MR, Arya AV, et al. Optical coherence tomography: a new tool for glaucoma diagnosis. *Curr Opin Ophthalmol*. 1995;6:89–95.

11. Costello F, Coupland S, Hodge W, et al. Quantifying axonal loss after optic neuritis with optical coherence tomography. *Ann Neurol*. 2006;59:963–969.
12. Talman L, Bisker E, Sacket D, et al. Longitudinal study of vision and retinal nerve fiber layer thickness in multiple sclerosis. *Ann Neurol*. 2010;67:749–760.
13. Skau M, Sander B, Milea D, Jensen R. Disease activity in idiopathic intracranial hypertension: a 3-month follow-up study. *J Neurol*. 2011;258:277–283.
14. Skau M, Milea D, Sander B, Wegner M, Jensen R. OCT for optic disc elevation in idiopathic intracranial hypertension. *Graefes Arch Clin Exp Ophthalmol*. 2011;249:723–730.
15. Wang JK, Kardon RH, Kupersmith MJ, Garvin MK. Automated quantification of volumetric optic disc swelling in papilledema using spectral-domain optical coherence tomography. *Invest Ophthalmol Vis Sci*. 2012;53:4069–4075.
16. Garvin M, Abràmoff M, Kardon R, Russell S, Wu X, Sonka M. Intraretinal layer segmentation of macular optical coherence tomography images using optimal 3-D graph search. *IEEE Trans Med Imaging*. 2008;27:1495–1505.
17. Friedman D, McDermott M, Kieburtz K, et al.; for the NORDIC IIHTT Study Group. The Idiopathic Intracranial Hypertension Treatment Trial (IIHTT): design considerations and methods. *J Neuroophthalmol*. 2014;34:107–117.
18. Mwanza J, Oakley J, Budenz D, Anderson D. Cirrus optical coherence tomography normative database study group: ability of Cirrus HD-OCT optic nerve head parameters to discriminated normal from glaucomatous eyes. *Ophthalmology*. 2011;118:241–248.
19. Kupersmith M, Sibony P, Mandel G, Durbin M, Kardon R. Optical coherence tomography of the swollen optic nerve head: deformation of the peripapillary RPE layer in papilledema. *Invest Ophthalmol Vis Sci*. 2011;52:6558–6564.
20. Sibony P, Kupersmith M, Rohlf FJ. Geometric morphometrics of the peripapillary SD-OCT: shape analysis of the RPE layer in papilledema and ischemic optic neuropathy. *Invest Ophthalmol Vis Sci*. 2011;52:7987–7995.
21. Domalpally A, Blodi B, Scott IU, et al.; for the SCORE Study Investigator Group. The standard care vs corticosteroid for retinal vein occlusion (SCORE) study system for evaluation of optical coherence tomograms. *Arch Ophthalmol*. 2009;127:1461–1467.
22. Costa R, Calucci D, Skaf M, et al. Optical coherence tomography 3: automatic delineation of the outer neural retinal boundary and its influence on retinal thickness measurements. *Invest Ophthalmol Vis Sci*. 2004;45:2399–2406.
23. Ishikawa H, Piette S, Liebmann J, Ritch R. Detecting the inner and outer borders of the retinal nerve fiber layer using optical coherence tomography. *Graefes Arch Clin Exp Ophthalmol*. 2002;240:362–371.
24. Wu Z, Vazeen M, Varma R, Sadda S. Factors associated with variability in retinal nerve fiber layer thickness measurements obtained by optical coherence tomography. *Ophthalmology*. 2007;114:1505–1512.
25. Ray R, Stinnett S, Jaffe G. Evaluation of image artifact produced by optical coherence tomography of retinal pathology. *Am J Ophthalmol*. 2005;139:18–29.
26. Sadda S, Wu Z, Walsh A, et al. Errors in retinal thickness measurements obtained by optical coherence tomography. *Ophthalmology*. 2006;113:285–293.
27. Keltner, J, Cello K, Balcer L, Calabresi P, Markowitz C, Werner JS. Stratus OCT quality control in two multi-centre multiple sclerosis clinical trials. *Neuroophthalmol*. 2011;35:57–64.
28. Wall M, White W. Asymmetric papilledema in idiopathic intracranial hypertension: prospective interocular comparison of sensory visual function. *Invest Ophthalmol Vis Sci*. 1998;39:134–142.
29. Kirkham T, Saunders M, Sapp G. Unilateral papilledema in benign intracranial hypertension. *Can J Ophthalmol*. 1973;8:533–538.
30. Huna-Baron R, Landau K, Rosenberg M, Warren F, Kupersmith MJ. Unilateral swollen disc due to increased intracranial pressure. *Neurology*. 2001;56:1588–1590.
31. El-Dairi M, Holgado S, O'Donnell T, Buckley E, Asrani S, Freedman S. Optical coherence tomography as a tool for monitoring pediatric pseudotumor cerebri. *J AAPOS*. 2007;11:564–570.

Appendix

OCT Substudy Committee (All Authors)

Peggy Auinger, MS (University of Rochester School of Medicine & Dentistry, Rochester, NY, USA), Mary Durbin, PhD (Carl Zeiss Meditec, Inc., Dublin, CA, USA), Steven Feldon, MD, MBA (University of Rochester School of Medicine & Dentistry, Rochester, NY, USA), Mona Garvin, PhD (University of Iowa, Iowa City, IA, USA), Randy Kardon, MD, PhD, (University of Iowa, Iowa City, IA, USA), John Keltner, MD (University of California, Davis, CA, USA), Mark Kupersmith, MD (OCT Principal Investigator, Roosevelt Hospital and New York Eye and Ear Infirmary, NY, NY, USA), Patrick Sibony, MD (State University of New York at Stony Brook, NY, USA), Kim Plumb (University of California, Davis, CA, USA), Jui-Kai Wang, MS (University of Iowa, Iowa City, IA, USA), John S. Werner, PhD (University of California, Davis, CA, USA)

IIHTT Acknowledgment List

Steering Committee: Michael Wall, MD (Principal Investigator, University of Iowa), James Corbett, MD, FAAN (University of Mississippi Medical Center), Steven Feldon, MD, MBA (University of Rochester Eye Institute), Deborah Friedman, MD (UT Southwestern Medical Center), John Keltner, MD (UC Davis Medical Center), Karl Kieburtz, MD, MPH (University of Rochester School of Medicine & Dentistry), Mark Kupersmith, MD (Network Chair) (Roosevelt Hospital), Michael P. McDermott, PhD (University of Rochester School of Medicine & Dentistry), Eleanor B. Schron, PhD, RN, FAAN (Project Officer, National Eye Institute), David Katz, MD (Bethesda Neurology LLC), Tippi Hales (Raleigh Neurology Associates PA), Cindy Casaceli, MBA (University of Rochester School of Medicine & Dentistry)

Substudy Sites: New York Eye and Ear Infirmary: Rudrani Banik, MD (Principal Investigator), Sanjay Kedhar, MD (Subinvestigator), Flora Levin, MD (Investigator), Jonathan Feistmann, MD (Investigator), Katy Tai, MA (Coordinator), Alex Yang, BA (Co-coordinator), Karen Tobias, BA (Coordinator), Melissa Rivas, BA (Co-coordinator), Lorena Dominguez, BA (Coordinator), Violete Perez, BA (Coordinator); University of Iowa and Department of Veterans Affairs: Reid Longmuir, MD (Principal Investigator), Matthew Thurtell, MBBS, MSc (Subinvestigator), Trina Eden (Coordinator), Randy Kardon, MD, PhD (Subinvestigator); The Eye Care Group: Robert Lesser, MD (Principal Investigator), Yanina O'Neil, MD (Subinvestigator), Sue Heaton, BS, CCRC (Coordinator), Nathalie Gintowt (Co-coordinator); Bascom Palmer Eye Institute, University of Miami: Byron L. Lam MD (Principal Investigator), Joshua Pasol MD (Subinvestigator), Potyra R. Rosa MD (Coordinator), Alexis Morante MS (Co-coordinator), Jennifer Verriotto MS (Coordinator); Bethesda Neurology, LLC: David Katz, MD (Principal Investigator), Tracy Asbury (Coordinator), Robert Gerwin, MD (Subinvestigator), Mary Barnett (Data Entry); Swedish Medical

Center: Steven Hamilton, MD (Principal Investigator), Caryl Tongco (Coordinator), Beena Gangadharan (Co-coordinator), Eugene May, MD (Subinvestigator); Dean A. McGee Eye Institute: Anil Patel, MD (Principal Investigator), Bradley Farris, MD (Subinvestigator), R. Michael Siatkowsk, MD (Subinvestigator), Heather Miller, LPN (Coordinator), Vanessa Bergman (Co-coordinator), Kammerin White (Coordinator), Steven O'Dell (Lumbar Puncture), Joseph Andrezik (Lumbar Puncture), Timothy Tytle (Lumbar Puncture); University of Pennsylvania: Kenneth Shindler MD, PhD (Principal Investigator), Joan Dupont (Coordinator), Rebecca Salvo (Coordinator), Sheri Drossner (Co-coordinator), Susan Ward (Coordinator), Jonathan Lo (Coordinator), Stephanie Engelhard (Coordinator), Elizabeth Windsor (Coordinator), Sami Khella (Lumbar Puncture), Madhura Tamhankar, MD (Subinvestigator); Washington University in St. Louis School of Medicine: Gregory Van Stavern, MD (Principal Investigator), Jamie Kambarian (Coordinator), Renee Van Stavern, MD (Subinvestigator), Karen Civitelli (Regulatory), J. Banks Shepherd, MD (Subinvestigator); University of Alabama Birmingham: Michael Vaphiades, DO (Principal Investigator), Jason Swanner, MD (Investigator), A. Blane Jett (Coordinator), Karen Searcey (Coordinator), Frankie Webb (Coordinator), Ashley Knight, BA (Coordinator), Shereka Lewis, BS (Coordinator), Lanning Kline, MD (Subinvestigator), Ronald Braswell, MD (Subinvestigator); Raleigh Neurology Associates, PA: Syndee J. Givre, MD, PhD (Principal Investigator), Tippi Hales (Coordinator), Penni Bye (Coordinator), Keisha Fuller (Coordinator), Kenneth M. Carnes, MD, (Subinvestigator), Kimberly James (Regulatory), Marisol Ragland (Data Entry); Saint Louis University: Sophia M. Chung, MD (Principal Investigator), Dawn M. Govreau, COT (Coordinator), John T. Lind, MD, MS (Subinvestigator); University of Rochester Eye Institute: Zoe Williams, MD (Principal Investigator), George O'Gara (Coordinator), Kari Steinmetz (Coordinator), Mare Perevich (Coordinator), Karen Skrine (Coordinator), Elisabeth Carter (Coordinator), Rajeev Ramchandran, MD (Subinvestigator); Ohio State University: Steven Katz, MD (Principal Investigator), Marc Criden, MD (Investigator), Gina Coman, RMA, CPC, OCS (Co-coordinator), John McGregor, FACS, MD, (Subinvestigator), Andrea Inman (Regulatory); Johns Hopkins University: Prem S. Subramanian, MD, PhD (Principal Investigator), Paul N. Hoffman, MD, PhD (Investigator), Marianne Medura (Coordinator), M. Michaele Hartnett (Coordinator), Madiha Siddiqui (Coordinator), Diane Brown (Coordinator), Ellen Arnold (Co-coordinator), Jeff Boring, MD (Subinvestigator), Neil R. Miller, MD (Subinvestigator); University of Southern California: Peter Quiros, MD (Principal Investigator), Sylvia Ramos (Coordinator), Margaret Padilla (Coordinator), Lupe Cisneros (Coordinator), Anne Kao, MD (Subinvestigator), Carlos Filipe Chicani, MD (Subinvestigator), Kevin Na (Regulatory); University of Houston: Rosa Tang, MD, MPH, MBA (Principal Investigator), Laura Frishman, PhD (Coordinator), Priscilla Cajavilca, MD (Coordinator), Sheree Newland, LVN (Coordinator), Liat Gantz, OD, PhD (Coordinator), Maria Guillermo Prieto, MD (Coordinator), Anastas Pass, OD, JD (Coordinator), Nicky R. Holdeman, OD, MD (Subinvestigator); University of Calgary: William Fletcher, MD, FRCPC (Principal Investigator), Suresh Subramaniam, MSc, MD, FRCPC (Investigator), Jeannie Reimer (Coordinator), Jeri Nickerson (Coordinator), Fiona Costello, MD, FRCPC (Subinvestigator); The Greater Baltimore Medical Center: Vivian Rismondo-Stankovich, MD (Principal Investigator), Maureen Flanagan, CO, COA (Coordinator), Allison Jensen, MD (Subinvestigator); State University of New York at Stony Brook: Patrick Sibony, MD (Principal Investigator), Ann Marie Lavorna, RN (Coordinator), Mary Mladek, COT (Coordinator), Ruth Tenzler, RN (Coordinator), Robert Honkanen, MD (Subinvestigator), Jill Miller-Horn, MD, MS (Lumbar Puncture), Lauren Krupp, MD (Lumbar Puncture); Massachusetts Eye and Ear Infirmary: Joseph Rizzo, MD (Principal Investigator), Dean Cestari, MD (Subinvestigator), Neal Snebold, MD (Investigator), Brian Vatcher (Coordinator), Christine Matera (Coordinator), Edward Miretsky, BA (Coordinator), Judith Oakley, BA (Coordinator), Josyane Dumser (Coordinator), Tim Alperen, BA (Coordinator), Sandra Baptista-Pires (Coordinator), Ursula Bator, OD (Coordinator), Barbara Barrett, RN (Coordinator), Charlene Callahan (Coordinator), Sarah Brett (Coordinator), Kamella Zimmerman (Coordinator), Marcia Grillo (Coordinator), Karen Capaccioli (Coordinator); Duke Eye Center and Duke University Medical Center: M. Tariq Bhatti MD (Principal Investigator), LaToya Greene, COA, CRC (Coordinator), Maria Cecilia Santiago-Turla (Coordinator), Noreen McClain (Coordinator), Mays El-Dairi MD (Subinvestigator); Florida State University College of Medicine: Charles Maitland, MD (Principal Investigator), H. Logan Brooks Jr, MD (Investigator), Ronda Gorsica (Coordinator), Brian Sherman, MD (Subinvestigator), Joel Kramer, MD (Subinvestigator); William Beaumont Hospital: Robert Granadier, MD (Principal Investigator), Tammy Osentoski, RN (Coordinator), Kristi Cumming, RN (Coordinator), Bobbie Lewis, RN (Coordinator), Lori Stec, MD (Subinvestigator)

Dietary Weight Loss Program: Betty Kovacs, Richard Weil, MEd, CDE, Xavier Pi-Sunyer, MD (New York Obesity Nutrition Research Center)

Fundus Reading Center: William Fisher, Dorothea Castillo, Valerie Davis, Lourdes Fagan, Rachel Hollar, Tammy Keenan, Peter MacDowell (University of Rochester Eye Institute)

Visual Reading Field Center: John Keltner, MD, Kim Plumb, Laura Leming, (UC Davis Department of Ophthalmology & Vision Science); Chris Johnson (University of Iowa)

Optical Coherence Tomography Reading Center: John Keltner, MD, John S. Werner, PhD, Kim Plumb, Laura Leming (UC Davis Department of Ophthalmology & Vision Science); Danielle Harvey, PhD (UC Davis Department of Public Health Sciences, Division of Biostatistics)

Data Coordination & Biostatistics Center: Jan Bausch, BS, Shan Gao, MS, Xin Tu, PhD (Biostatistics); Debbie Baker, Deborah Friedman, MD, MPH (Medical Monitor), Karen Helles, Nichole McMullen, Bev Olsen, Larry Preston, Victoria Snively, Ann Stoutenburg (CHET/CTCC) (University of Rochester School of Medicine & Dentistry)

NORDIC Headquarters: O. Iyore Ayanru, Elizabeth-Ann Moss, Pravin Patel (Roosevelt Hospital)

Consultant: Richard Mills, MD (Glaucoma Consultants Northwest)

Data Safety Monitoring Board Members: Maureen Maguire, PhD (Chair, University of Pennsylvania), William Hart Jr, MD, PhD, Joanne Katz, ScD, MS (Johns Hopkins), David Kaufman, DO (Michigan State University), Cynthia McCarthy, DHCE MA, John Selhorst, MD (Saint Louis University School of Medicine)

Adjudication Committee: Kathleen Digre, MD (University of Utah); James Corbett, MD, FAAN (University of Mississippi Medical Center); Neil R. Miller, MD (Johns Hopkins University); Richard Mills, MD (Glaucoma Consultants Northwest)

Investigative Ophthalmology & Visual Science